ELSEVIER

Dynamics of Atmospheres and Oceans
35 (2002) 205–225

dynamics of atmospheres and oceans

www.elsevier.com/locate/dynatmoce

Laboratory modeling of topographic Rossby normal modes

Stefano Pierini [a,*], Adam M. Fincham [b], Dominique Renouard [b], Maria Rosaria D'Ambrosio [c], Henry Didelle [b]

[a] *Dipartimento di Fisica (INFM), Università dell'Aquila, Via Vetoio, 67010 Coppito (AQ), Italy*
[b] *Coriolis, LEGI-UJF-CNRS 21, Av. Martyrs, 38000 Grenoble, France*
[c] *I.I.A.S.S. "E.R. Caianiello", Via G. Pellegrino, 19-84019 Vietri sul Mare (SA), Italy*

Received 26 October 2000; accepted 15 November 2001

Abstract

The physical modeling of topographic Rossby normal modes carried out at the "Coriolis" Rotating Platform (Grenoble), is presented. The basic feature of the bottom topography is a linear slope of 4.3 m × 2 m delimited by two lateral walls. Since the studied motions are essentially barotropic, homogeneous water was used. Unsheared currents were generated by a simple movement of a wavemaker located in front of the topographic barrier. The conservation of potential vorticity for the currents flowing onto the channel slope produced Rossby waves: reflections at the lateral boundaries then led to the formation of propagating barotropic Rossby normal modes, whose frequencies and spatial structures were selected by the physical system. The currents were measured through the correlation imaging velocimetry (CIV) method, which allowed an extremely detailed synoptic map of the horizontal velocities in an area ($\sim$13 m^2) including the slope to be obtained every 30 s.

A variety of experiments were performed in order to provide a complete process study in which the effect of different channel lengths and rotation periods could be tested. Two different lengths of the linear slope, 4.3 and 3.3 m, and rotation periods ranging from 30 to 50 s were considered. The qualitative analysis of the 2D current patterns, and the good agreement found between the measured eigenperiods and the periods obtained by means of a simple analytical model, show that in all cases the first Rossby normal mode was generated. Moreover, numerical simulations based on the shallow-water equations, for a geometry and paddle movements that match closely the experimental setup, allow to calibrate the analytical model and provide useful information on a discrepancy found between experimental and analytical eigenperiods due to an oscillation of the normal mode trajectory.

Keywords: Rossby normal modes; Laboratory modeling; Correlation imaging velocimetry; Shallow-water numerical modeling

* Corresponding author. Tel.: +39-862-433-033; fax: +39-862-433-081.
E-mail address: stefano.pierini@aquila.infn.it (S. Pierini).

0377-0265/02/$ – see front matter
PII: S0377-0265(02)00002-7

1. Introduction

Rossby waves are ubiquitous dynamical features in the oceans. They are barotropic or baroclinic rotational waves owing their existence to the restoring force provided by the planetary or topographic β-effect (e.g. Pedlosky, 1987). Planetary Rossby waves (i.e. those related to the variation of the Coriolis parameter with latitude) account for an important part of the wind-driven subinertial variability over spatial scales of O(100–1000 km). Barotropic waves can have very small periods of O(10–100 days) while baroclinic waves at mid-latitudes have a lower cutoff period of O(1 year). Multiple reflections at horizontal boundaries can give rise to planetary Rossby normal modes (PRMs), with a discrete set of eigenperiods dependent on the geometry of the basin. On the other hand topographic Rossby waves (i.e. those supported by an equivalent topographic β-effect) have much smaller space and time scales, since they are confined over strong topographic slopes, typically with spatial scales of O(100 km), and have periods that can be just above the inertial one. Also for topographic Rossby waves multiple reflections due to both coasts and sharp topographic variations can lead to the excitation of topographic Rossby normal modes (TRMs).

PRMs contribute to shape the high frequency barotropic variability of large oceans. Willebrand et al. (1980) showed in a numerical study that in the north Atlantic the characteristic time scale of dissipation is larger than the time necessary for a barotropic Rossby wave to propagate westward across the basin for the 4–5 lowest basin modes, so that they may be excited, with periods ranging from 10 to 15 days. Pierini (1990, 1997) showed that in fact these modes can be in equilibrium with the wind without any substantial westward intensification, while for higher forcing periods the forced response is in terms of westward intensified Rossby modes (Pierini, 1998). In the Atlantic Ocean PRMs have never been unambiguously observed while in the Pacific Ocean Luther (1982) showed persuasive evidence of a 4–6 days PRM with an energy *e*-folding time of less than 3 days. The effect of the mid-ocean ridge on the structure of PRMs was considered by Barnier (1984), Matano (1995), Pedlosky and Spall (1999), and Pedlosky (2000).

TRMs (e.g. Ripa, 1978) are fundamental elements in the theory of long-period tides (e.g. Wunsch, 1967; Platzman et al., 1981; Carton, 1983; Miller et al., 1993), determining locally the structure of the tidal response. However, only very recently experimental and numerical evidence was provided suggesting that such dynamical features can play an important role in coastal oceanography. While topographic Rossby *waves* have been clearly identified in various oceanic sites (e.g. Thompson, 1971; Thompson and Luyten, 1976; Okkonen, 1993), in a study on the circulation over the ridge connecting Iceland to the Faeroe islands, Miller et al. (1996) gave for the first time unambiguous experimental evidence of a TRM. Both the experimental eigenperiod 1.8 days and the corresponding spatial structure of the mode were satisfactorily explained by a shallow-water model. Pierini (1996) applied a barotropic circulation model to the central Mediterranean Sea and showed that TRMs with periods ranging from 2 to 5 days can be excited in the Strait of Sicily by both wind anomalies and remote barotropic flows produced by pressure fluctuations on a basin scale. Theoretical evidence that TRMs can be excited in the Mediterranean Sea is also provided by Candela and Lozano (1994). In general, because of their small periods, the possible existence of TRMs in several oceanographic sites might not be revealed in residual current signals simply because the modes may be filtered out together with the tidal currents. It is therefore

possible that topographic Rossby modes could be more ubiquitous than is usually believed, also in view of their ability to be excited easily by different forcing agents (Pierini, 1996). Assessing this hypothesis would be relevant as far the understanding of horizontal mixing in regions of bounded topographic slopes is concerned, as it was pointed out (Pierini and Zambianchi, 1995), that—due to their particular dynamical nature—TRMs can produce chaotic advection of passive tracers.

As far as laboratory studies are concerned, simulations in rotating tanks to model topographic Rossby waves have been carried out (e.g. Sommeria et al., 1991), but the combined process of Rossby wave generation, wave reflection at horizontal boundaries and consequent excitation of normal modes has not received much attention. Only Pedlosky and Greenspan (1967) and Beardsley (1975) have conducted analytical, laboratory and numerical investigations into the role of TRMs in the "sliced cylinder" model. Further physical modeling of TRMs could shed light on their generating and propagating mechanisms and, at the same time, it could be useful for validating numerical studies. Moreover, the physical modeling of TRMs over a linear slope would of course be equivalent to modeling PRMs. The "Coriolis" Rotating Platform in Grenoble was in this respect an ideal and unique experimental facility. The physical modeling of TRMs was in fact carried out at "Coriolis" with the support of the "Large-Scale Facilities Programme" of the European Commission. In this paper, we present the results of these experimental investigation, along with a numerical validation through the use of a mathematical model.

In Section 2 the experimental setup, the generating mechanism used to produce TRMs, and the measuring techniques (in particular the correlation imaging velocimetry, i.e. CIV) that have allowed the flows to be monitored are described. In Section 3 a basic experiment is presented in detail. From this discussion the dynamical mechanism that leads to TRM excitation is revealed. In Section 4 sensitivity experiments are presented corresponding to different rotation rates and channel lengths. In all cases the obtained TRM eigenperiods are compared to an analytical formula and good agreement is found. Finally, in Section 5 numerical experiments performed by means of a shallow-water numerical model are presented and their comparison with the experimental results is discussed.

2. The experimental setup and the measuring techniques

The experimental setup and the generating mechanism to be implemented in the "Coriolis" rotating tank was suggested by a numerical study concerning the Strait of Sicily. Pierini (1996) showed that TRMs with periods ranging from 2 to 5 days can be excited over the complex topographic pattern resembling a ridge between Tunisia and Sicily by two different forcing agents that are essentially equivalent. First of all the wind can induce such motions through the interaction with the local topography of remote currents associated with wind stress anomalies, rather than (as suggested by Miller et al., 1996) through a local resonant interaction with the atmospheric forcing. Secondly, similar current variations induced remotely through open boundaries without any wind forcing produce the same results. In other terms the relative vorticity required by the TRM, instead of being transferred locally by a wind stress curl, is induced through the conservation of potential vorticity by a current (even originally irrotational) flowing over the ridge. These considerations suggest a way

of generating TRMs in the laboratory and, in turn, the actual excitation of these motions would support the hypothesis that this can be an effective generating mechanism.

2.1. Experimental setup

In view of these considerations the topography of Fig. 1a was adopted. Two regions of different depth (0.6 and 0.3 m) were connected by a linear slope of 4.3 m × 2 m delimited by two walls necessary to provide the Rossby wave reflections required for the excitation of the normal modes (in the analogy with the Strait of Sicily the outer boundary would represent the western Sicilian coasts and the inner one the Tunisian coasts). The external boundary was made movable in order to allow for different slope lengths. Since the studied motions are essentially barotropic, homogeneous water was used. A topographic correction that takes into account the surface curvature due to the centrifugal force was also introduced.

According to the aforementioned discussion on the Strait of Sicily TRM generation, horizontally and vertically unsheared currents were generated by a large paddle that moved toward the slope with a simple time dependence, an example of which is given in Fig. 1b. As we will see in the following sections, the conservation of potential vorticity for the flow impinging over the channel slope produces topographic Rossby waves: reflections at the lateral boundaries then lead to the formation of propagating barotropic Rossby normal modes, whose frequencies and spatial structures are selected by the physical system. It is worth noticing that during its motion the paddle generates a couple of strong vortical motions just behind it. In this respect the motion "toward" the slope had the advantage that the paddle (which at the end of its motion was very close to the edge of the slope) acted as a shield that prevented such vortices from contaminating the signal to be studied. In the various experiments the rotation rate ranged from 30 to 50 s and slope lengths of 4.3 and 3.3 m were considered.

2.2. Correlation imaging velocimetry

In the first set of experiments the flows were measured by means of a series of eight sonic currentmeters located in four points along the central isobath of the slope. This made it possible to identify the propagation of Rossby waves by observing the phase lag between different points, and allowed for a rough evaluation of the eigenperiods. Unfortunately, in this set of experiments the paddle was moved "away" from the slope (unlike in the experiments presented in this paper), so that the shielding effect of the paddle was absent (see Section 2.1), and the vortices produced by the paddle motion introduced a relatively large noise in the time series.

For a subsequent set of experiments the currentmeters were removed and the CIV technique was implemented in the 13 m^2 region delimited by the rectangle "B" that includes the slope in Fig. 1a (that is by far the largest area ever used for a measuring technique of this kind) in order to monitor synoptically the induced flows. CIV is a highly accurate imaging velocimetry technique that relies on the cross-correlation of local areas of image texture between two images taken a short time apart Δt_{CIV} (details of the algorithms and optimization procedures can be found in Fincham and Spedding, 1997). Such techniques do not rely on the use of particle images, and in principle, any passive tracer that provides image

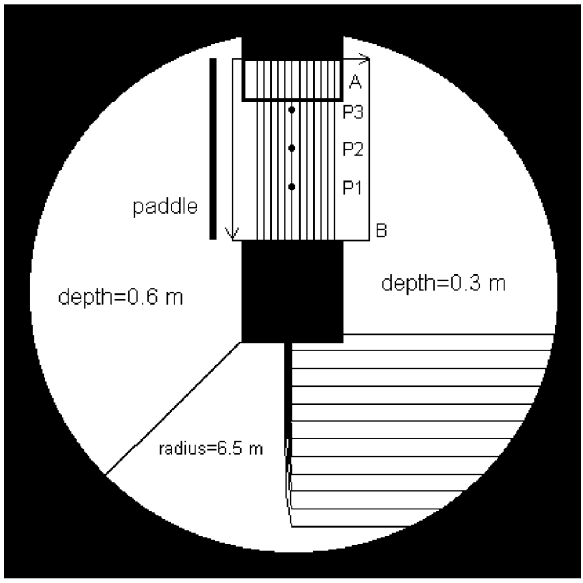

(a)

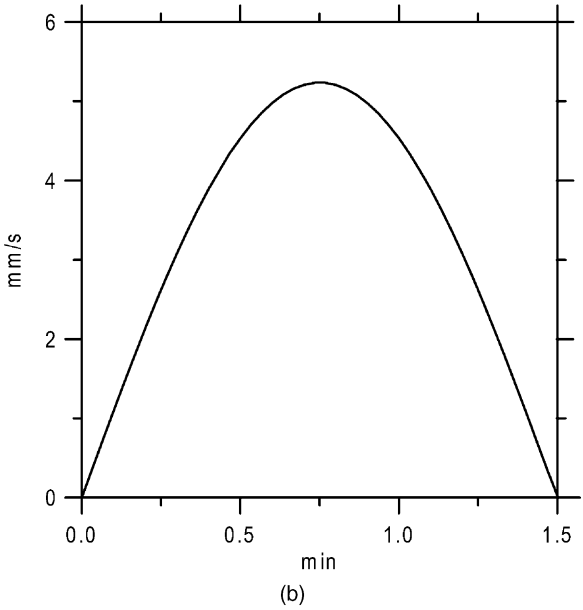

(b)

Fig. 1. (a) The experimental setup showing a plan view of depths in the circular tank, the working region is the rectangle denoted “B” at the top; (b) example of time dependence of the paddle velocity.

texture and follows the flow may be used. Measurements over large areas in homogeneous fluids require large neutrally buoyant tracers. Small drops of fluorescence dye dissolved in common salt solution were sprinkled over the measurement surface before each experiment. These slightly heavier drops of dye descend through the fluid depth forming a dyed turbulent wake that quickly dissipates leaving behind a fossilized column of dye of neutral buoyancy. When illuminated by a horizontal sheet of laser light, highly textured images are produced. CIV divides each image into smaller pattern boxes containing sufficient image texture, these boxes are then correlated with the same region in the second image and the peak of the spatial correlation function determines the displacement of the tracer pattern. The raw velocity data from each image pair is subjected to both automatic and manual verifications before being re-interpolated onto a regular grid. This re-interpolation is done using a thin shell smoothing spline (Spedding and Rignot, 1993). The divergence of the velocity field and the vorticity can also be computed after this smoothing. In this respect a byproduct of the interpolation process is that the spatial derivatives can be computed directly from the spline coefficients and, in order to suppress grid-scale fluctuations a 4th order butterworth spectral filter is applied before computation of the spatial derivatives.

In our case the sheet of laser light was produced at a depth of 15 cm, the image resolution was 768 pixels × 484 pixels, Δt_{CIV} ranged from 3 to 10 s and a sample every 30 s was obtained, so that the evolution of the flow in all its stages could be followed in real time.

3. A basic experiment

A variety of experiments were performed in order to provide a complete process study in which the effect of different channel lengths and rotation periods could be tested. In this section, we present and discuss an experiment (exp. A) that puts in evidence all the main aspects of the dynamics (the other experiments will be presented in the next section). In exp. A (Table 1), the rotation period was taken as $T_{\mathrm{rot}} = 45$ s, the largest slope length ($L_x = 4.3$ m) was used and the speed of the paddle is the one shown in Fig. 1b (at $t = 0$ the fluid was virtually in solid body rotation, with a very small superimposed residual motion). The paddle approached the limit of the slope covering a length of 0.3 m, and the final position was 44 mm away from it. The choice of such a simple paddle movement ensures that any oscillations arising over the slope are due to dynamical mechanisms intrinsic of the system and do not depend on the details of the forcing mechanism. This generating mechanism can

Table 1
List of the experiments referred to in the text identified by their rotation period and slope length[a]

Experiment	T_{rot} (s)	L_x (m)	T_{sp} (min)	T_0 (min)	T_{num} (min)
A	45	4.3	∼2.5	2.70	∼2.7
B	35	4.3	∼2	2.10	–
C	50	4.3	∼3	3.00	–
D	35	3.3	∼2.5	2.35	–
E	45	3.3	∼2.8	3.03	∼3

[a] T_{sp} are the experimental eigenperiods, T_0 the eigenperiods obtained by Eq. (1), and T_{num} are the eigenperiods obtained by solving numerically model (2).

therefore be thought of as the simplest possible one that introduces a perturbation in a fluid in solid body rotation in the presence of a topographic ridge.

Fig. 2 shows eight snapshots of velocities measured with CIV taken every 30 s starting from $t = 0.5$ min (Fig. 2a) in the domain represented by the rectangle "B" in Fig. 1a (the orientation of the x- and y-axis is indicated by the arrows of rectangle B, in particular the lower boundary corresponds to the one facing the paddle). The images a, b and c show flows during the forced phase. They exhibit the response over the topographic β-plane (given by the slope) to an irrotational current impinging orthogonally to the isobaths (the irrotational character of the flow is lost over the slope and even in its vicinity, as shown near the lower boundary, because of the interaction with the sloping bottom). Negative relative vorticity is induced through the conservation of potential vorticity as soon as the water columns put in motion by the paddle reach the bottom slope. In Fig. 2a this is evidenced by the formation of an anticyclonic gyre extending over the whole slope. In the flow patterns 2b and c this feature is accompanied by the "westward" (leftward) propagation of topographic Rossby waves. In Fig. 2c (corresponding to the instant at which the paddle stops) the anticyclonic gyre has squeezed near the left boundary and a cyclonic gyre has taken its place in the middle of the slope.

From now on (Fig. 2d–h and Fig. 3) the evolution is free, and the typical structure of the first Rossby normal mode is evident (two main gyres of opposite sign propagating along lines of constant planetary vorticity). Pedlosky (1987, Section 3.25) shows how this can be achieved by means of the superposition of four appropriate plane waves produced by lateral reflections in a closed rectangular domain. In our case, although the slope is unbounded in the direction normal to the isobaths, the lines of topographic gradient discontinuity along which the slope is connected with the regions of flat bottom act as "equivalent" coasts as far as the Rossby wave reflections are concerned. The further evolution (Fig. 3) evidences a dissipation of energy due basically to bottom friction and also to the eddy viscosity associated with the production of small eddies near the lateral boundaries that subtract energy from the coherent Rossby normal mode. Moreover, an oscillation in the "trajectory" of the normal mode can be noticed starting from 2.5 min (Fig. 2e). Possible implications related to this behavior will be discussed in Section 5.

In Fig. 4 the time series of the y-component of the velocities, $-v$ in points P1, P2, and P3 of Fig. 1 are reported. They are computed from the CIV currents of Figs. 2 and 3 by averaging over circles of 25 cm radius. The phase lag between the three points is due to the leftward propagation, and in each point an oscillation with a period of $T_A \approx 2.5 \pm 0.1$ min can be computed empirically from the graph of Fig. 4. Such period is by no means related to the time history of the paddle movement (different movements of the paddle produced the same period), but it is rather selected by the dynamical system and can therefore be considered as the eigenperiod of the first Rossby normal mode excited by the interaction of the current produced by the paddle with the geometry and topography of the ridge.

It is useful to consider the simple analytical model for the first Rossby normal mode in a closed rectangular β-plane as a reference for a quantitative interpretation of the obtained T_A. The lowest eigenperiod is given by (Pedlosky, 1987):

$$T_0 = T_{rot}\pi L_x \frac{D_0}{D - D_1}\sqrt{\frac{1}{L_x^2} + \frac{1}{(\delta L_y)^2}}, \qquad D_0 = \frac{D + D_1}{2} \tag{1}$$

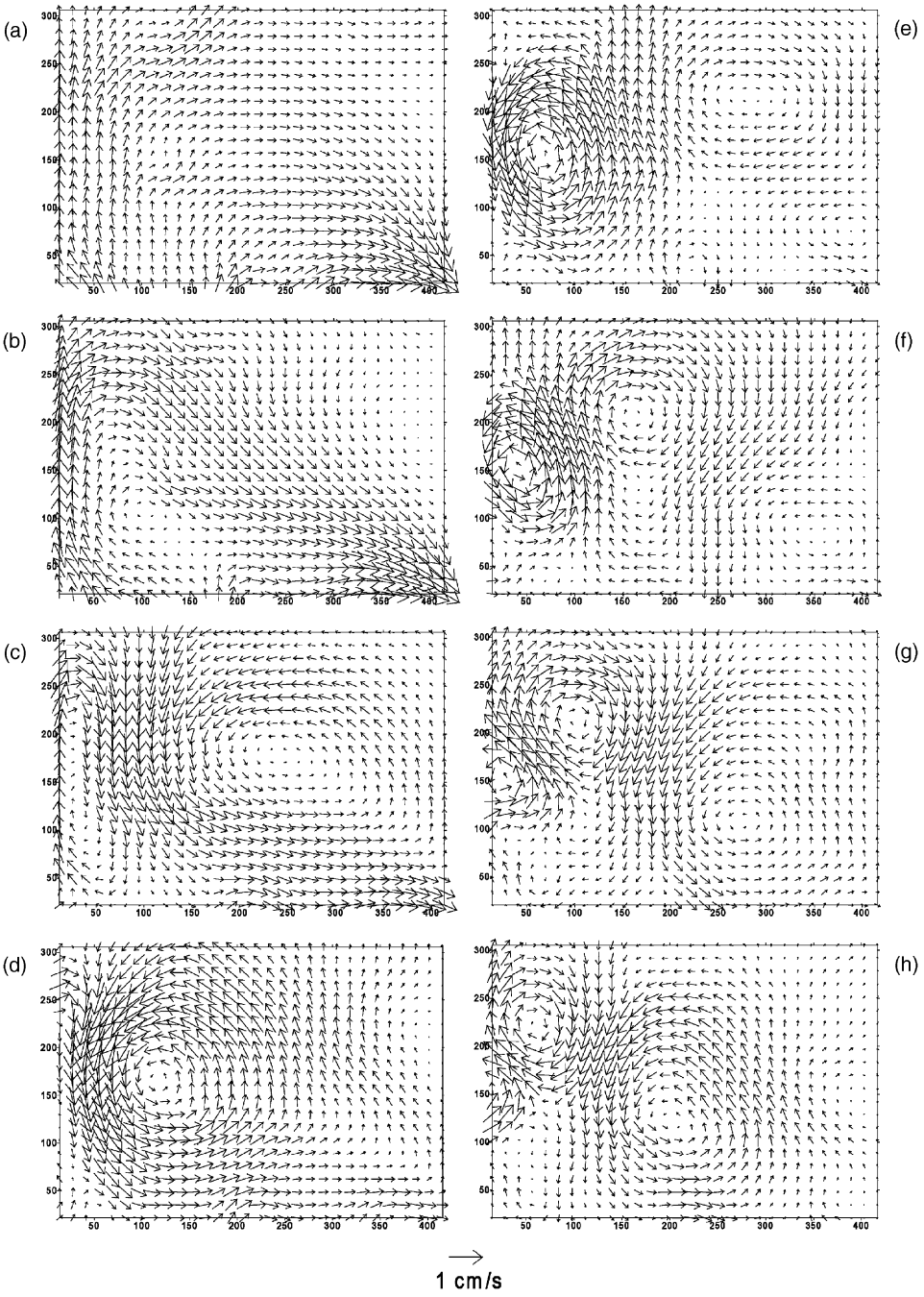

Fig. 2. Velocities measured by the CIV for exp. A. Parts a–h correspond to $t = 0.5, 1, \ldots, 4$ min. Axis units are in cm, with orientation as shown in Fig. 1a (the paddle is situated below the long (x) axis).

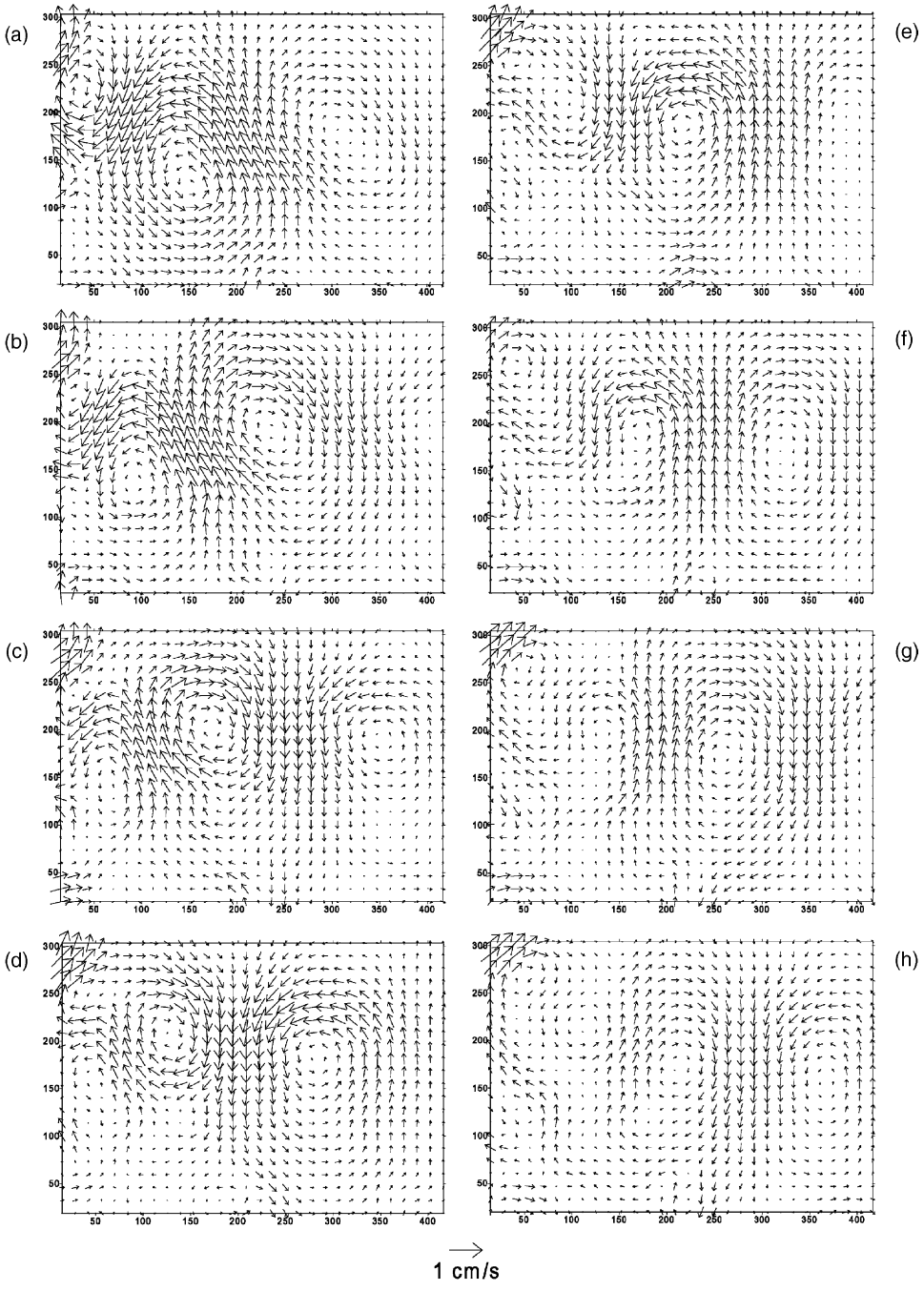

Fig. 3. Velocities measured by the CIV for exp. A. Parts a–h correspond to $t = 4.5, 5, \ldots, 8$ min. Axis units are in cm.

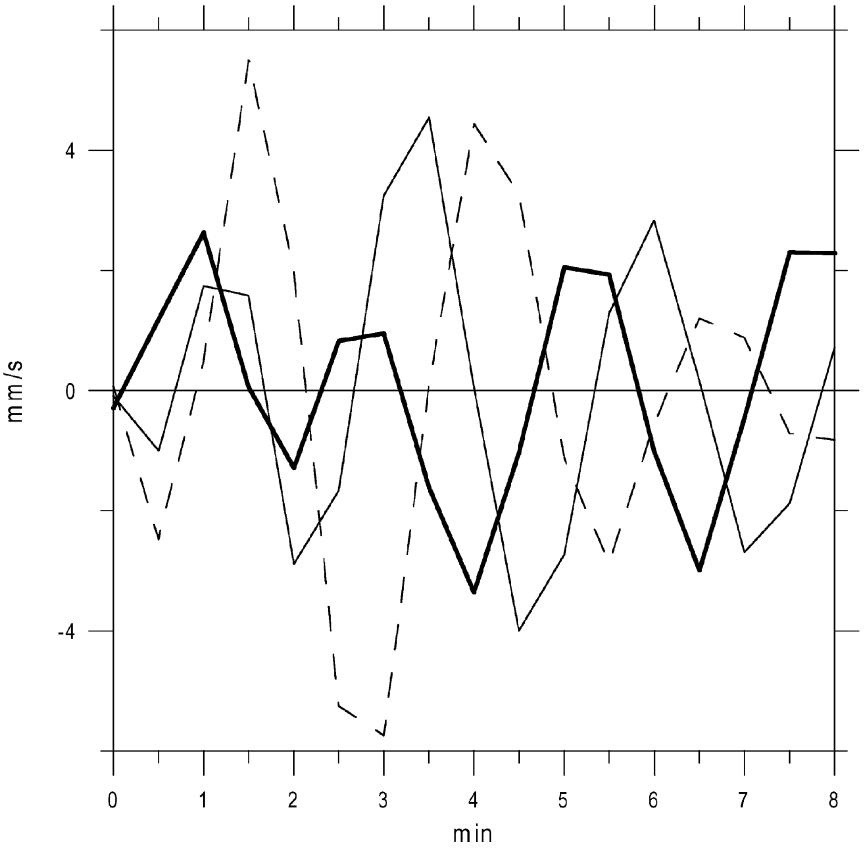

Fig. 4. Cross-isobath CIV velocities averaged over circles of 25 cm radius centered in points P1 (thick solid line), P2 (solid line), and P3 (dashed line) for exp. A.

where the planetary β-effect is substituted by the equivalent topographic β-effect of the bottom slope ($D = 0.6$ m is the depth of the deep region, $D_1 = 0.3$ m that of the shallow region, and D_0 a mean water depth at the slope), L_x and L_y are the two linear dimensions of the sloping channel ($L_x = 4.3$ m, $L_y = 2$ m) and δ is a non-dimensional parameter introduced in order to take into account departures from the closed rectangular β-plane model. With these values and $\delta = 1$ one gets $T_{0A} = 3.9$ min.

A better agreement with $T_A \approx 2.5$ min can be obtained if a correction $\delta > 1$ to L_y is introduced in order to empirically take into account the fact that, due to the lack of rigid boundaries along y, the motions extend all over the 3 m $\times$ 4.3 m rectangle covered by the CIV apparatus, as it is evident from Figs. 2 and 3. The parameter δ should therefore have a value $\delta \approx 1.5$, for an effective $L_y \approx 3$ m. We will see in Section 5 that a numerical shallow-water model simulates well the observed motion of experiment A, apart from a residual motion present only in the laboratory experiments. As a consequence, the value $T_{numA} \approx 2.7$ min (see Section 5) produced by the numerical simulation is expected to be

described by Eq. (1) even more accurately then it is for the experimental eigenperiod T_A, therefore δ can be chosen so as to give $T_{0A} = T_{numA}$. As a consequence, we will choose here, and for all the experiments described in the next section, the value $\delta = 1.65$ (for an effective $L_y = 3.3$ m) which gives $T_{0A} = T_{numA} = 2.7$ min (see Table 1).

It should be noticed that T_{0A} overestimates T_A by ∼8%. One should consider that the analytical model (1) does not represent accurately the experimental setup, as other differences cannot be empirically taken into account, such as the non-constant value of the topographic β-effect over the 3 m × 4.3 m rectangle (since it is constant over the 2 m × 4.3 m slope region but is zero outside), or the absence of rigid boundaries along x. Moreover, in Section 5 we will analyze a further reason that can account for part of the discrepancy between experimental and analytical eigenperiods. Nonetheless, the comparison of the experimental eigenperiod with the period given by Eq. (1) provides a good quantitative validation (in addition to the qualitative validation given above) of the hypothesis that the induced oscillations are associated with the first TRM.

4. Sensitivity experiments

In this section we discuss experiments that differ from exp. A both as far as the rotation period T_{rot} and the slope length L_x are concerned. Experiments B and C (see Table 1 and Fig. 5) differ from exp. A in that the rotation period is now 35 and 50 s, respectively, the time dependence of the paddle movement being still given by Fig. 1b. While at $t = 1$ min, i.e. still during the forced phase, the response is very similar for both experiments, the free evolution shows a clear difference in the normal mode eigenperiod. In Fig. 6 the time series of $-v$ in point P2 for experiments B, A and C (corresponding to rotation periods of 35, 45, and 50 s, respectively) are reported. We have already discussed the agreement between the experimental eigenperiod and the analytical estimate provided by Eq. (1) for exp. A in the preceding section. For exps. B and C with the same values used for A but with the appropriate T_{rot} one gets from Eq. (1): $T_{0B} = 2.10$ min and $T_{0C} = 3$ min, in very good agreement with the experimental eigenperiods deducible from the graph of Fig. 6: $T_B \approx 2$ min and $T_C \approx 3$ min.

In the next two experiments, D and E (see Table 1), the length of the slope L_x was reduced from 4.3 to 3.3 m by moving the outer boundary 1 m toward the center of the tank (so that the boundary is now given by the thick solid line "A" of Fig. 1a). Fig. 7 shows the responses for exp. D (a–d) and exp. E (a′–d′), which are qualitatively similar to those of the previous experiments, but now for the same T_{rot} one has larger eigenperiods, as implied by Eq. (1) (exps. B and A correspond to exps. D and E, respectively, the only difference being the length L_x). The theoretical eigenperiods given by Eq. (1) are: $T_{0D} = 2.35$ min and $T_{0E} = 3.03$ min. These values are once more in good agreement with the experimental ones deducible from the graph of Fig. 8, where $-v$ in P2 is plotted as a function of time for the two experiments: $T_D \approx 2.5$ min and $T_E \approx 2.8$ min. The comparison between the time series in P2 for the experiments that were performed with the same T_{rot} but with different slope lengths (exps. A and E) are reported in Fig. 9, in which therefore the effect of varying L_x is put in evidence. In conclusion, the agreement between the eigenperiods computed by formula (1) for all the experiments performed (differing by T_{rot} and L_x) and the

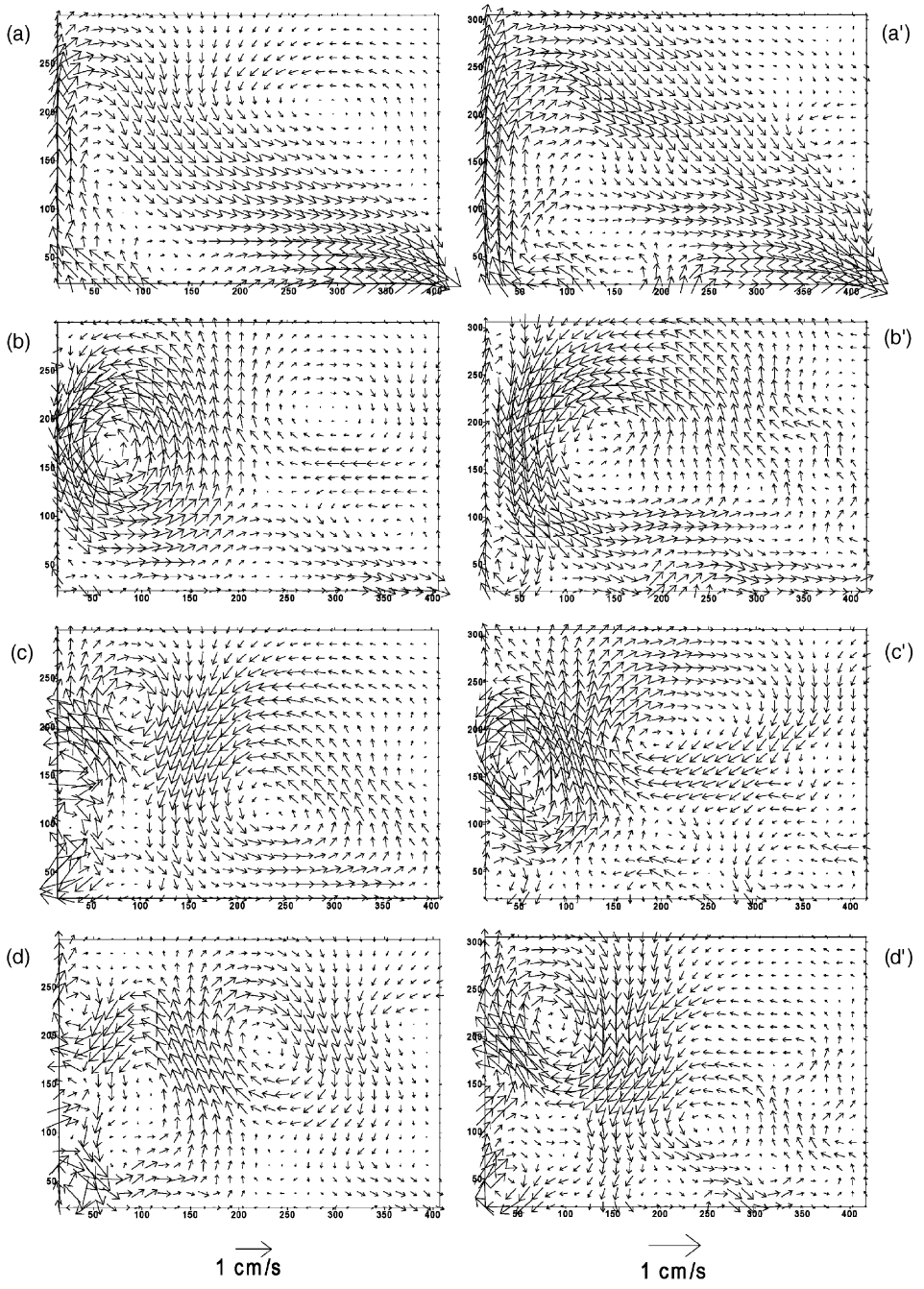

Fig. 5. Velocities measured by the CIV for exp. B (a, b, c, and d: $t = 1, 2, 3, 4$ min) and for exp. C (a′, b′, c′, and d′: $t = 1, 2, 3, 4$ min). Axis units are in cm.

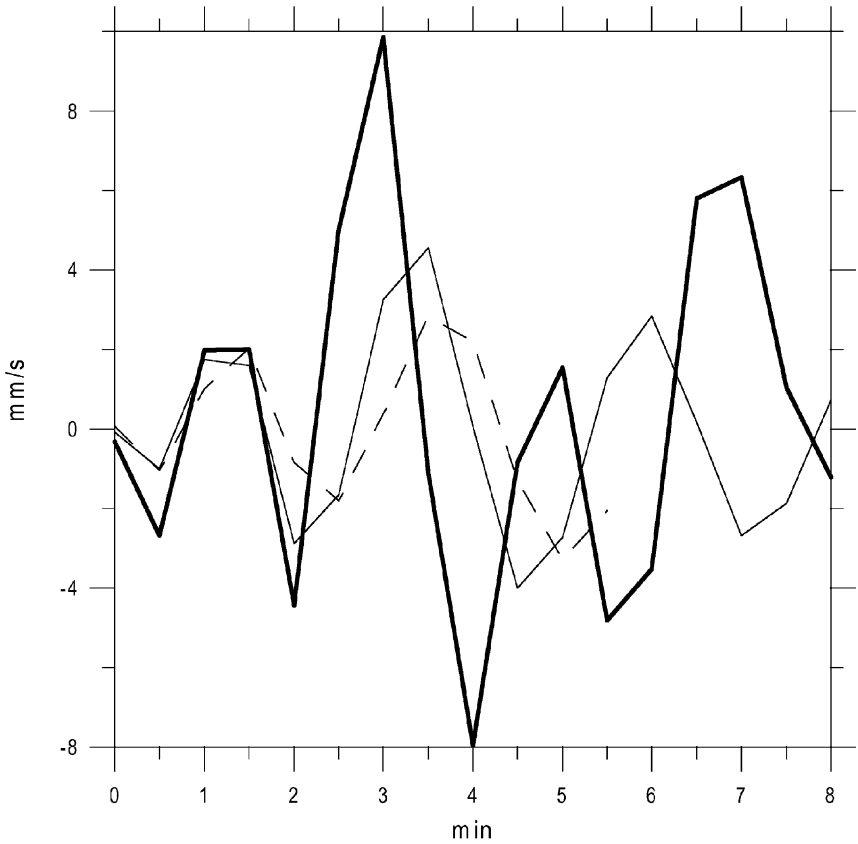

Fig. 6. Cross-isobath CIV velocities averaged over a circle of 25 cm radius centered in point P2 for experiments B (thick solid line), A (solid line), and C (dashed line), corresponding to $T_{\mathrm{rot}} = 35, 45, 50$ s, respectively.

observed periods of the oscillations indicate that we are actually observing the generation and subsequent evolution of the first topographic Rossby normal mode.

5. Mathematical modeling of the observed flows

Along with the laboratory experiments, the mathematical modeling of the studied motions was carried out. It was based on the non-linear shallow-water equations for a homogeneous incompressible fluid (e.g. Pedlosky, 1987):

$$\boldsymbol{u}_t + (\boldsymbol{u}\cdot\nabla)\boldsymbol{u} + f\boldsymbol{k}\times\boldsymbol{u} = -g\nabla\eta + \frac{\tau_{\mathrm{b}}}{\rho H} + A_H\nabla^2\boldsymbol{u}, \qquad \eta_t + \nabla(H\boldsymbol{u}) = 0 \tag{2}$$

where $\boldsymbol{u}$ is the horizontal velocity, $\eta(x, y, t)$ the sea surface displacement, f the Coriolis parameter, $\boldsymbol{k} = (0, 0, 1)$, g the acceleration of gravity, ρ the water density, $H = D + \eta(x, y, t) - d(x, y)$ where D is the maximum water depth and $d(x, y)$ the bottom relief, $\tau_{\mathrm{b}} = \rho C_{\mathrm{Db}}|\boldsymbol{u}|\boldsymbol{u}$

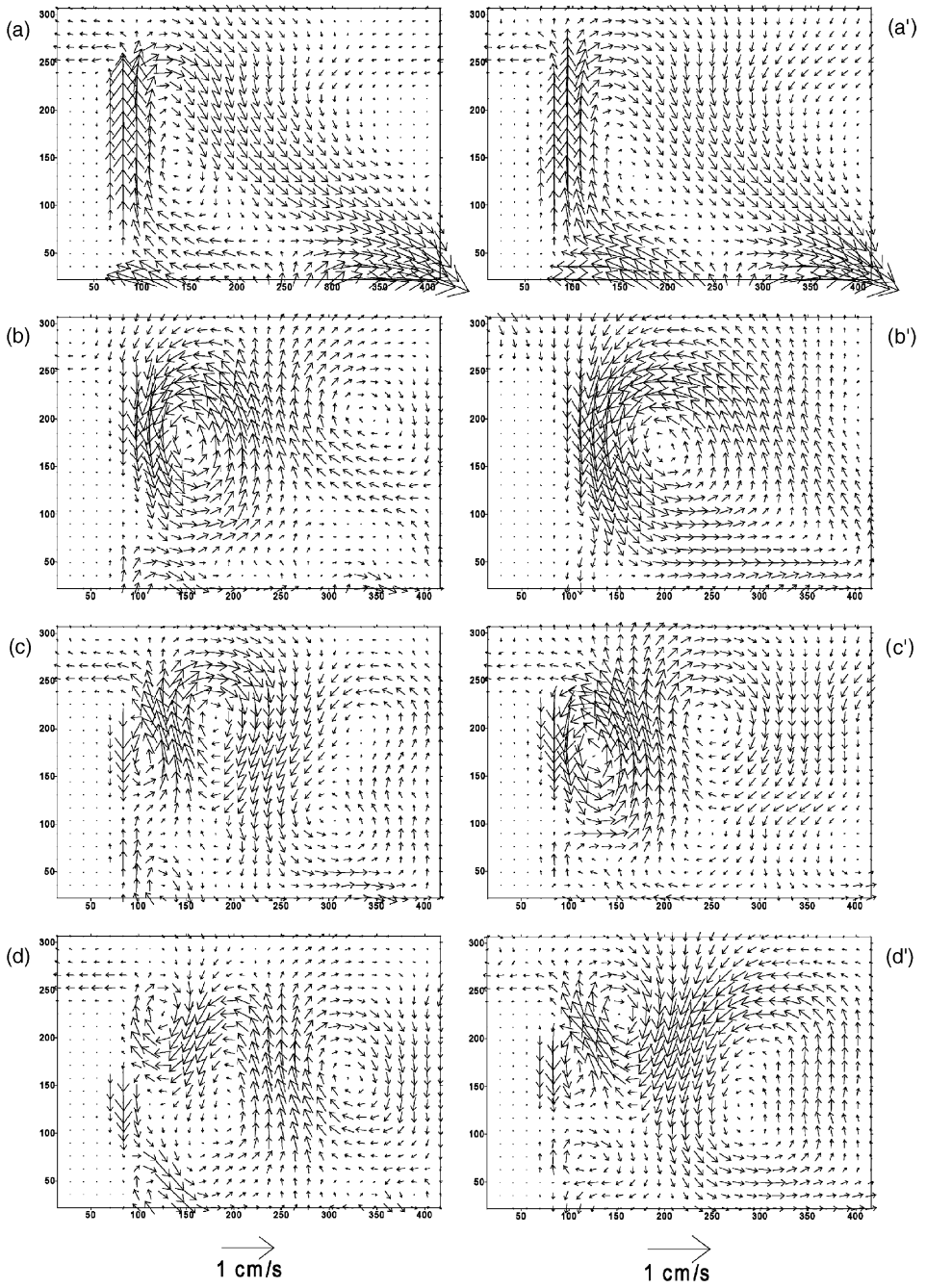

Fig. 7. Velocities measured by the CIV for exp. D (a, b, c, and d: $t = 1, 2, 3, 4$ min) and for exp. E (a′, b′, c′, and d′: $t = 1, 2, 3, 4$ min). Axis units are in cm.

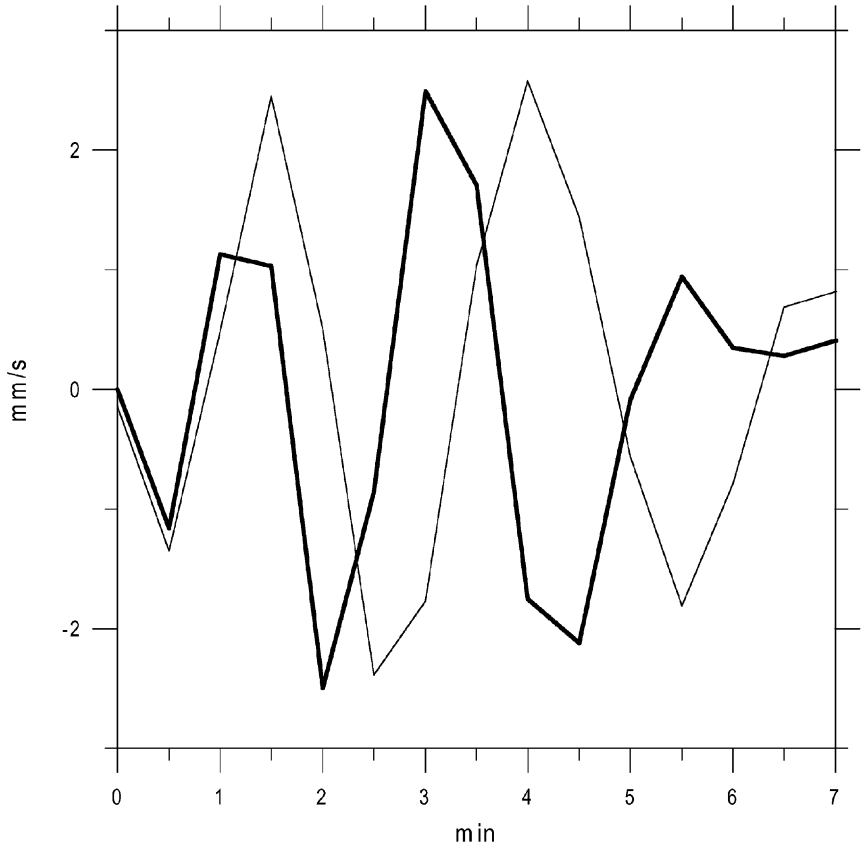

Fig. 8. Cross-isobath CIV velocities averaged over a circle of 25 cm radius centered in point P2 for experiments D (thick solid line) and E (solid line), corresponding to $T_{\mathrm{rot}} = 35, 45$ s, respectively.

the bottom stress and A_H the lateral eddy viscosity coefficient. A finite difference scheme on the Arakawa C-grid was used to solve the mathematical model numerically (Pierini, 1996) in a geometric environment that resembles closely the experimental setup. The paddle motion is simulated by imposing a velocity normal to the paddle profile, with the same time dependence as the one of the real paddle (Fig. 1b). The grid spacing is $\Delta x = \Delta y = 20$ cm, the time step $\Delta t = 0.01$ s and the dissipating parameters are $A_H = 0.001\ \mathrm{m}^2/\mathrm{s}$ and $C_{\mathrm{Db}} = 0.002$.

In Figs. 10 and 11 experimental and numerical results for experiments A and E (differing only in the slope length) are compared in a window given by the rectangle "B" of Fig. 1a. The two fields are in excellent agreement (especially during the forced phase), and all the main dynamical features are well reproduced by the numerical model. However, two notable differences are evident. First of all the decrease of current amplitudes is more pronounced in the numerical signal than in the experimental one. This is due to the relatively large value of the horizontal eddy viscosity necessary in the numerical model to damp unresolved scales and strictly related to the spatial resolution. In the numerical model this effect is more

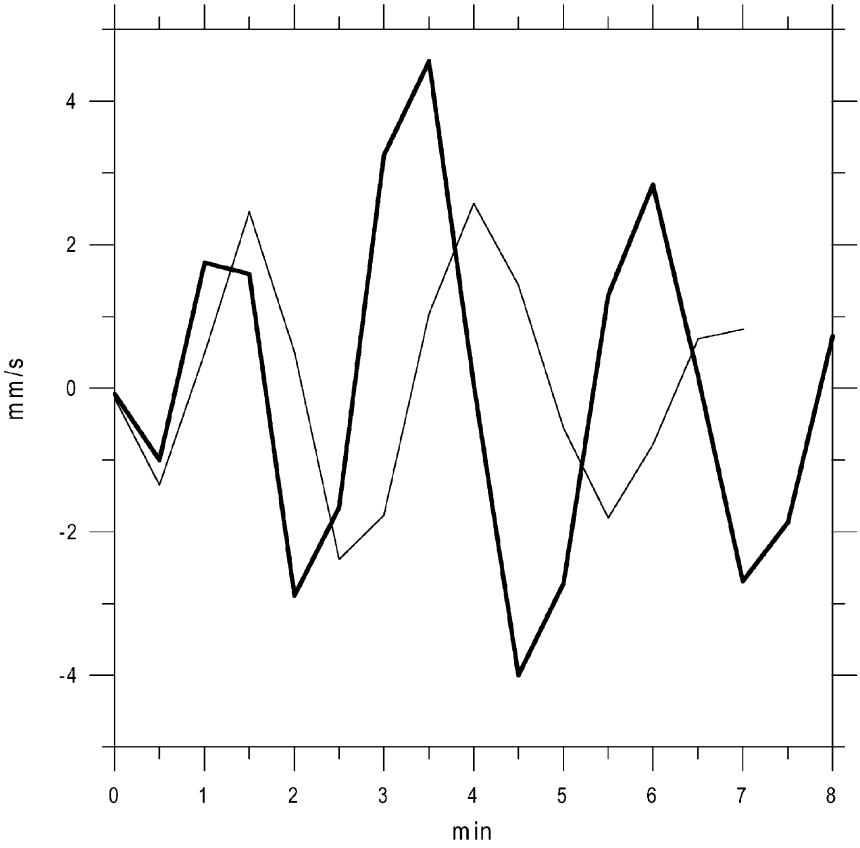

Fig. 9. Cross-isobath CIV velocities averaged over a circle of 25 cm radius centered in point P2 for experiments A (thick solid line) and E (solid line), corresponding to $T_{\mathrm{rot}} = 45$ s for the long and reduced slope length, respectively.

important than the bottom friction, while the latter appears to be the predominant dissipative mechanism in the experiments, apart from regions close to the lateral boundaries. Naturally, a higher resolution model could produce a slower energy decay, in better agreement with the experiments. The second difference concerns the eigenperiods. The "numerical" ones, as computed from the graphs of Fig. 12, are $T_{\mathrm{numA}} \approx 2.7$ min, $T_{\mathrm{numE}} \approx 3$ min. They match the analytical eigenperiods $T_{0\mathrm{A}}$ and $T_{0\mathrm{E}}$ given by Eq. (1) because the value of δ was tuned (Section 3) just for this purpose (but it should be stressed that the resulting value $\delta = 1.65$ corresponds well to the observed spatial distribution of energy, as discussed in Section 3). However, these values are larger than the experimental eigenperiods by ∼8%.

How can this small discrepancy be explained? An oscillation in the trajectory of the normal mode is evident in Figs. 10c and 11c and, even more clearly, in Figs. 2, 3, 5 and 7. The consequence is an increase of the length of the ray path, and therefore a decrease of the experimental eigenperiod with respect to the normal mode produced by the numerical

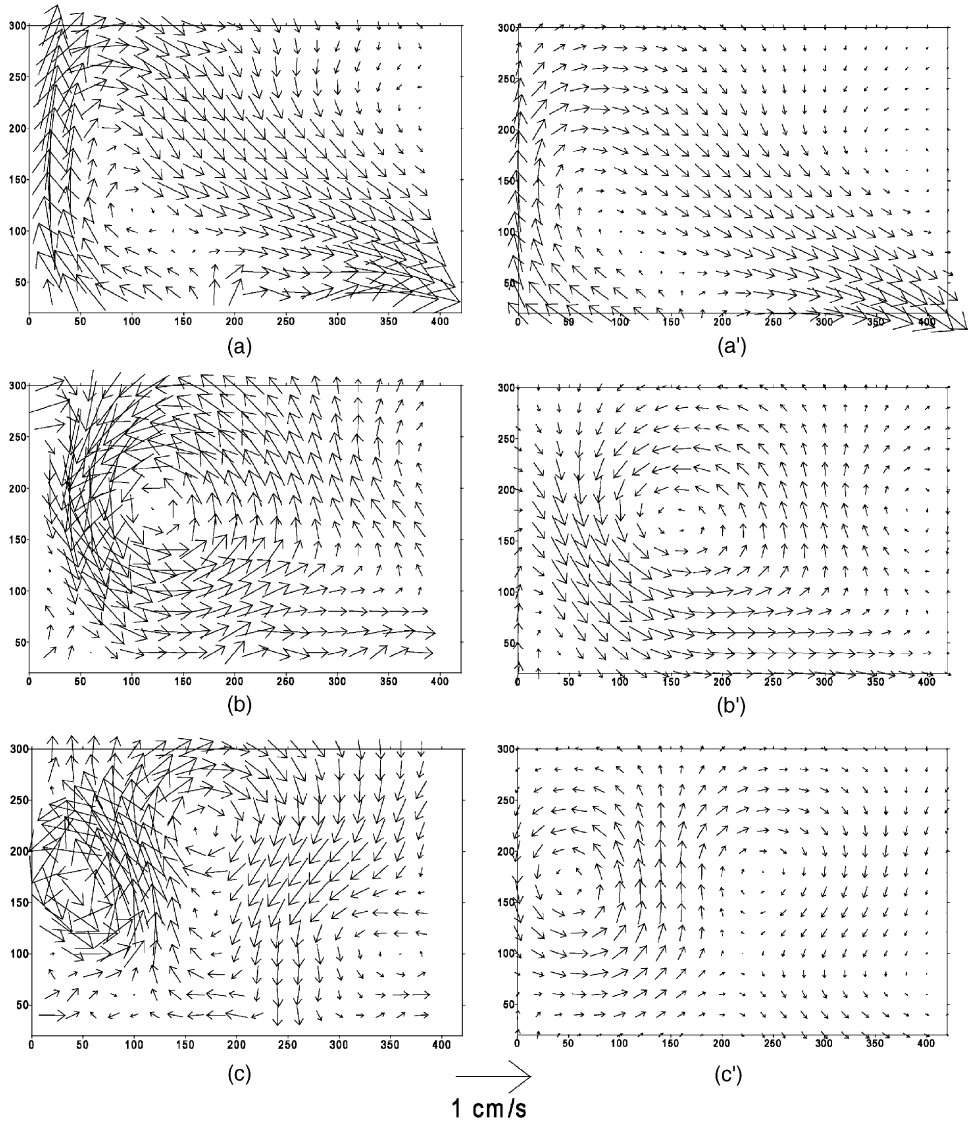

Fig. 10. Exp. A (a, b, and c): velocities measured by the CIV and interpolated onto a regular 20 cm × 20 cm grid at times $t = 1, 2, 3$ min, respectively; (a′, b′, and c′): velocities computed by the numerical model on a regular 20 cm × 20 cm grid at times $t = 1, 2, 3$ min, respectively. Axis units are in cm.

simulation, in which such an oscillation is absent (Figs. 10c′ and 11c′). This can account for the small discrepancy noticed earlier. It can be conjectured that the oscillation is related to some form of instability of the normal mode to small perturbations (for instance associated with small asymmetries in the paddle motion) that are present in the real experiment but not in the numerical model. The instabilities would be limited by the effect of the

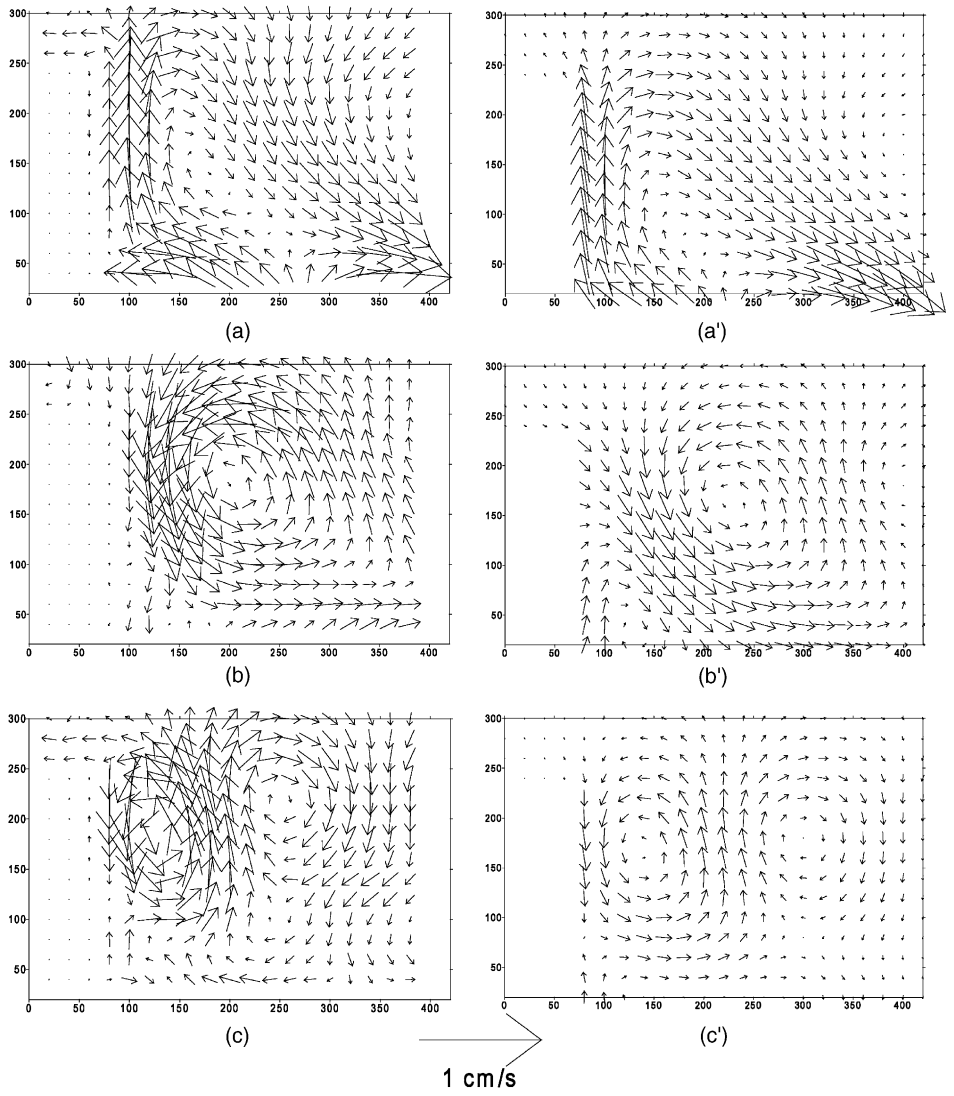

Fig. 11. Exp. E (a, b, and c): velocities measured by the CIV and interpolated onto a regular 20 cm × 20 cm grid at times $t = 1, 2, 3$ min, respectively; (a′, b′, and c′) velocities computed by the numerical model on a regular 20 cm × 20 cm grid at times $t = 1, 2, 3$ min, respectively. Axis units are in cm.

topographic wave guide, in so maintaining the basic structure of the topographic Rossby normal mode. It is worth stressing that the use of the numerical model: (i) has allowed to tune the parameter δ in the analytical model (1), (ii) has contributed to identifying the dynamical nature of the observed motions, and (iii) has also allowed to isolate the trajectory oscillation from the overall normal mode structure and to estimate qualitatively its effect on the eigenperiod.

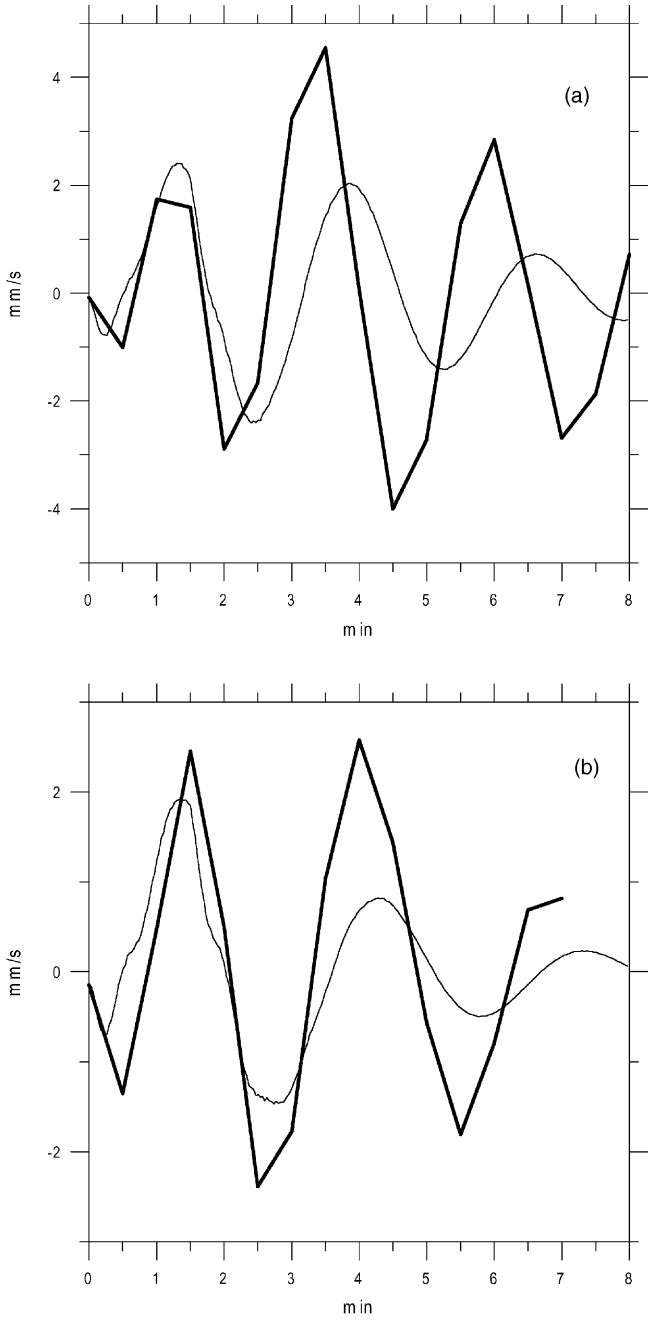

Fig. 12. (a) Exp. A; (b) exp. E. Thick lines: cross-isobath CIV velocities averaged over a circle of 25 cm radius centered in point P2; thin lines: cross-isobath velocities in point P2 computed numerically by means of model (2).

6. Conclusions

Topographic Rossby normal modes were successfully modeled in the "Coriolis" Rotating Platform. A numerical study on the excitation of these rotational oscillations in the Strait of Sicily (Pierini, 1996) suggested that they can be generated by the interaction of a large-scale current with the topography of a laterally bounded topographic slope. This in turn suggested that these modes could be excited in a rotating tank by means of an unsheared current produced by a simple motion of a paddle located in front of a bounded slope. The experiments have confirmed this conjecture. A variety of experiments were performed in order to provide a complete process study in which the effect of different channel lengths and rotation periods could be tested. The interpretation of the motions thus obtained in terms of first topographic Rossby normal modes was supported by both a qualitative analysis of the 2D current patterns of the currents measured by the CIV method, and by a quantitative analysis of the obtained eigenperiods by means of a simple analytical formula.

This experiment has contributed to clarify a scientific issue, and to evidence the importance of the use of the CIV measuring technique and of a numerical circulation model. As far as the scientific issue is concerned, the experiment has shown that a very effective generating mechanism of TRMs is the one given by the interaction of a large-scale current with a topographic slope in the presence of lateral boundaries, the characteristics of the current being not relevant in the process. This implies that rotational time-dependent motions of this kind could be ubiquitous dynamical features in sites of the world oceans that have similar geometrical characteristics and where, therefore, TRMs could contribute to the horizontal mixing through the mechanism of chaotic advection. As far as the CIV measuring technique is concerned, its application to the present experiment has allowed the verification of its ability to give extremely detailed and reliable synoptic information on the velocity field over an area which is by far the largest one ever used for a measuring technique of this kind. Moreover, the availability of frequent 2D velocity fields has proved invaluable for the identification of motions, such as TRMs, which have very specific spatial and temporal features. Finally, the use of a numerical circulation model implemented in a geometric environment that resembles closely the experimental setup has allowed to calibrate the analytical model, has contributed to identifying the dynamical nature of the observed motions, and has also allowed the isolation of an unexpected modulation observed in the trajectory of the normal mode from its overall structure, that deserves to be investigated in future studies.

Acknowledgements

The authors are most grateful to R. Carcel who helped in the experiments. This research was supported by the European Commission's Human Potential Programme, Transnational Access to Major Research Infrastructures and the European Commission project HYDRIV, Contract HPRI-199-50042.

References

Barnier, B., 1984. Influence of a mid-ocean ridge on wind-driven barotropic Rossby waves. J. Phys. Oceanogr. 14, 1930–1936.

Beardsley, R.C., 1975. The sliced-cylinder laboratory model of the wind-driven ocean circulation. Part 2. Oscillatory forcing and Rossby wave resonance. J. Fluid Mech. 69, 41–64.

Candela, J., Lozano, C.J., 1994. Barotropic response of the western Mediterranean to observed atmospheric pressure forcing. In: La Violette, P. (Ed.), Seasonal and interannual variability of the western Mediterranean Sea, Vol. 46. Coastal and Estuarine Studies. American Geophysical Union, Washington, DC, pp. 325–359.

Carton, J.A., 1983. The variation with frequency of the long-period tides. J. Geophys. Res. 88, 7563–7571.

Fincham, A.M., Spedding, G.R., 1997. Low-cost, high resolution DPIV for measurement in turbulent fluid flows. Exp. Fluids 23, 449–462.

Luther, D.S., 1982. Evidence of a 4–6 days barotropic, planetary oscillation of the Pacific Ocean. J. Phys. Oceanogr. 12, 644–657.

Matano, R.P., 1995. Numerical experiments on the effects of a meridional ridge on the transmission of energy by barotropic Rossby waves. J. Geophys. Res. 100 (18), 18271–18280.

Miller, A.J., Luther, D.S., Hendershott, M.C., 1993. The fortnightly and monthly tides: resonant Rossby waves or nearly equilibrium gravity waves? J. Phys. Oceanogr. 23, 879–897.

Miller, A.J., Lermusiaux, P.F.J., Poulain, P.M., 1996. A topographic-Rossby mode resonance over the Iceland–Faeroe ridge. J. Phys. Oceanogr. 26, 2735–2747.

Okkonen, S.R., 1993. Observations of topographic planetary waves in the Bering slope current using the Geosat altimeter. J. Geophys. Res. 98 (22), 22603–22613.

Pedlosky, J., 1987. Geophysical Fluid Dynamics. Springer-Verlag, New York.

Pedlosky, J., 2000. The transmission of Rossby waves through basin barriers. J. Phys. Oceanogr. 30, 495–511.

Pedlosky, J., Greenspan, H.P., 1967. A simple laboratory model for the oceanic circulation. J. Fluid Mech. 27, 291–304.

Pedlosky, J., Spall, M., 1999. Rossby normal modes in basins with barriers. J. Phys. Oceanogr. 29, 2332–2349.

Pierini, S., 1990. A divergent quasi-geostrophic model for wind-driven oceanic fluctuations in a closed basin. Dyn. Atmos. Oceans 14, 259–277.

Pierini, S., 1996. Topographic Rossby modes in the Strait of Sicily. J. Geophys. Res. 101, 6429–6440.

Pierini, S., 1997. Westward intensified and topographically modified planetary modes. J. Phys. Oceanogr. 27, 1459–1471.

Pierini, S., 1998. Wind-driven fluctuating western boundary currents. J. Phys. Oceanogr. 28, 2185–2198.

Pierini, S., Zambianchi, E., 1995. Dispersion mechanisms in quasi-geostrophic modes. In: Proceedings of the XXI General Assembly of International Association of the Physical Sciences of the Oceans (I.A.P.S.O.), Honolulu, Hawaii.

Platzman, G.W., Curtis, G.A., Hansen, K.S., Slater, R.D., 1981. Normal modes of the world ocean. Part II. Description of modes in the period range 8 to 80 hours. J. Phys. Oceanogr. 11, 579–603.

Ripa, P., 1978. Normal Rossby modes of a closed basin with topography. J. Geophys. Res. 83, 1947–1957.

Sommeria, J., Meyers, S.D., Swinney, H.L., 1991. Experiments on vortices and Rossby waves in eastward and westward jets. In: Osborne, A.R. (Ed.), Nonlinear Topics in Ocean Physics, Vol. CIX. International School of Physics Enrico Fermi, Elsevier, Amsterdam, pp. 227–269.

Spedding, G.R., Rignot, E.J.M., 1993. Performance analysis and application of grid interpolation techniques for fluid flows. Exp. Fluids 15, 417–430.

Thompson, R., 1971. Topographic Rossby waves at a site north of the Gulf Stream. Deep Sea Res. 18, 1–19.

Thompson, R., Luyten, J.R., 1976. Evidence for bottom-trapped topographic Rossby waves from single moorings. Deep Sea Res. 23, 629–635.

Willebrand, J., Philander, S.G.H., Pacanowski, R.C., 1980. The oceanic response to large-scale atmospheric disturbances. J. Phys. Oceanogr. 10, 411–429.

Wunsch, C., 1967. The long-period tides. Rev. Geophys. 5, 447–475.